

DOI:10.1002/ejic.201402084

# Probing the Influence of the Ligands on the Magnetism of Dinuclear Manganese, Iron, and Chromium Complexes Supported by Aroylhydrazone

Alex Domingo,<sup>\*,[a]</sup> David Specklin,<sup>[b]</sup> Vitor Rosa,<sup>[b,c]</sup>  
Samir Mameri,<sup>[b]</sup> Vincent Robert,<sup>[a]</sup> and Richard Welter<sup>[b]</sup>

**Keywords:** Magnetic properties / Transition metals / Metal–metal interactions / Ab initio calculations

The influence of aroylhydrazone and bridging ligands on the exchange coupling constant ( $J$ ) of five dinuclear metal complexes is analyzed through ab initio calculations. The complete active space second-order perturbation theory with localized orbitals offers not only estimates of  $J$  but also detailed information about the contributions of the molecular regions to the overall magnetism. This computational strategy is first validated for two previously reported ferromagnetic Mn<sup>III</sup>/Mn<sup>III</sup> and antiferromagnetic Fe<sup>III</sup>/Fe<sup>III</sup> complexes. Such cal-

culations are extended to three new dinuclear complexes of Mn<sup>IV</sup>, Fe<sup>III</sup> and Cr<sup>III</sup> constructed with a chemically simpler ligand (HL). We provide the synthesis and structural characterization (X-ray diffraction crystallography) of these three new compounds. The HL ligand exhibits little electronic influence over the  $J$  value, but it directs the magnetic properties of the compound by conditioning the relative arrangement of the metal centres.

## Introduction

The design of molecular materials with specific electromagnetic properties requires an understanding of the effect of the structure on the phenomenon of interest. In transition metal complexes, this knowledge has come a long way and, nowadays, powerful predictions based on the ligand field theory are at hand.<sup>[1]</sup> Nonetheless, small changes to the molecular structure can still introduce, exacerbate or even quench the macroscopic properties of such complexes. One of the fields in which this kind of relationship is of the most interest is molecular magnetism, for which the control of exchange magnetic couplings at the molecular scale is of unique significance. In recent decades, a class of complexes characterized by a small number of paramagnetic transition metal ions (<30) connected to each other by simple bridging anions, typically O<sup>2-</sup>, HO<sup>-</sup> or CH<sub>3</sub>O<sup>-</sup>, has provided valuable insights as simple models of more complex systems.<sup>[2]</sup> Prime examples are found in catalysis and biological processes, particularly in the case of Mn and Fe com-

pounds.<sup>[3]</sup> The intermetallic bridges of this class of compounds create a superexchange pathway that often leads to isotropic couplings and, in some cases, slow relaxation of the magnetization to make a so-called single-molecule magnet (SMM).<sup>[4]</sup> Such magnets are promising candidates for applications in molecular spintronics, high-density data storage and quantum information processing.<sup>[5]</sup> The discovery of SMMs of low nuclearity, down to four centres, stimulated the research effort on dinuclear complexes, the simplicity of which favours studies of structure–coupling–constant relationships and time-consuming theoretical calculations.

In recent years, an ongoing effort has been made to prepare a variety of transition metal compounds coordinated to aroylhydrazone ligands and analyze the effect of systematic structural alterations on the magnetic properties (Scheme 1).<sup>[6]</sup> As a result, it was shown that dinuclear Mn<sup>IV</sup>, Fe<sup>III</sup> and Cr<sup>III</sup> complexes bearing this type of ligand are antiferromagnetic.<sup>[7]</sup> Specifically, the Fe-based species proved to be of interest in solar energy conversion.<sup>[8]</sup> Furthermore, a dinuclear Mn<sup>III</sup>/Mn<sup>III</sup> complex displays the strongest ferromagnetic interaction reported to date between two bridged Mn<sup>III</sup> ions.<sup>[9]</sup>

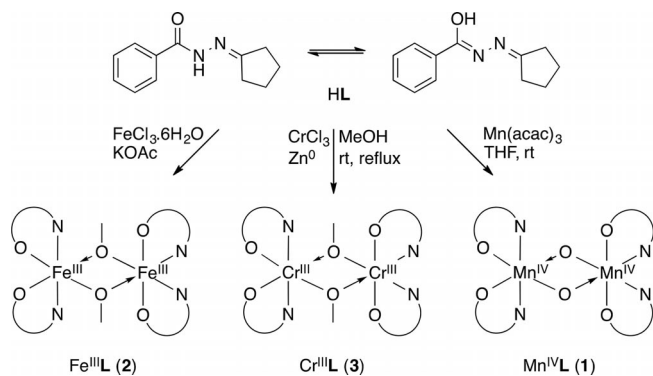
The aim of the present work is to gain further insight into the structural features that control the exchange coupling constant ( $J$ ) of dinuclear complexes based on aroylhydrazone ligands. We have developed a computational strategy based on ab initio multiconfigurational wave functions that is capable of unravelling the influence of particular regions of the molecule on the overall magnetism of the

[a] Laboratoire de Chimie Quantique, UMR 7177-CNRS/Unistra, Université de Strasbourg,  
1 rue Blaise Pascal, 67000 Strasbourg, France  
E-mail: domingo@unistra.fr  
http://quantique.u-strasbg.fr

[b] Laboratoire DECOMET, UMR 7177-CNRS/Unistra, Université de Strasbourg,  
4 rue Blaise Pascal, 67000 Strasbourg, France

[c] REQUIMTE, Departamento de Química, Faculdade de Ciências e Tecnologia, Universidade Nova de Lisboa, Caparica 2829-516, Portugal

Supporting information for this article is available on the WWW under <http://dx.doi.org/10.1002/ejic.201402084>.

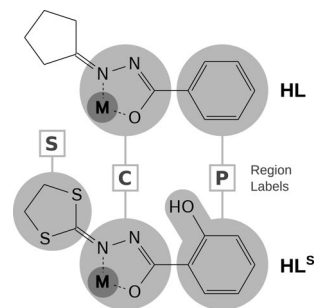


Scheme 1. Preparation of dinuclear Mn, Fe and Cr complexes (1–3) with the HL ligand.

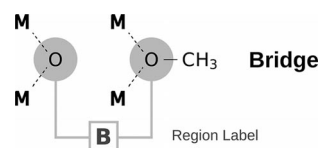
compound. The combination of the complete active space second-order perturbation theory (CASPT2) method,<sup>[10]</sup> which has proven to be very efficient for the treatment of electron correlation effects on transition metal compounds,<sup>[11]</sup> with localized molecular orbitals (MOs) allows us to enable or disable arbitrarily defined regions of the molecule.

We validated the proposed theoretical method through its application to two previously reported and fully characterized dinuclear complexes with the *N'*-(1,3-dithiolan-2-ylidene)-2-hydroxybenzohydrazide ( $\text{H}_2\text{L}^{\text{S}}$ ) ligand, namely,  $[\text{Mn}^{\text{III}}_2(\mu\text{-OMe})_2(\text{HL}^{\text{S}})_4]$  with a strong ferromagnetic character<sup>[9]</sup> and its analogue  $[\text{Fe}^{\text{III}}_2(\mu\text{-OMe})_2(\text{HL}^{\text{S}})_4]$  with an antiferromagnetic coupling.<sup>[7a]</sup> These two compounds will be referred to as  $\text{Mn}^{\text{III}}\text{HL}^{\text{S}}$  and  $\text{Fe}^{\text{III}}\text{HL}^{\text{S}}$ , respectively. Subsequently, the theoretical strategy was applied to a new series of three dinuclear complexes based on the ligand *N'*-cyclopentylidenebenzohydrazide (HL). The simpler chemical structure of the HL ligand in comparison to that of  $\text{H}_2\text{L}^{\text{S}}$  will help us to assess the effect of some functional groups on the ligand and the role of the basic aroyl-hydrazone structure. The three HL complexes are  $[\text{Mn}^{\text{IV}}_2(\mu\text{-O})_2(\text{L})_4]$ ,  $[\text{Fe}^{\text{III}}_2(\mu\text{-OMe})_2(\text{L})_4]$  and  $[\text{Cr}^{\text{III}}_2(\mu\text{-OMe})_2(\text{L})_4]$ , the synthesis and structural characterization of which are described herein. These three compounds will be referred to as  $\text{Mn}^{\text{IV}}\text{L}$ ,  $\text{Fe}^{\text{III}}\text{L}$  and  $\text{Cr}^{\text{III}}\text{L}$ , respectively.

The present evaluation of the magnetic properties of these five dinuclear compounds offers not only estimates of their *J* values but also detailed information about the contributions of different parts of the molecule to the overall magnetism. The partitioning scheme for the HL/ $\text{H}_2\text{L}^{\text{S}}$  ligands and the bridges, which was used to evaluate their influence on the molecular magnetism, is illustrated in Schemes 2 and 3. The inspections along the series of compounds with the HL ligand in combination with the data obtained from the two complexes with  $\text{H}_2\text{L}^{\text{S}}$  reveal clear common traits between them. The role of the dimetallic core and the bridges dominates the intermetallic exchange coupling constant. On the other hand, the HL and  $\text{H}_2\text{L}^{\text{S}}$  ligands have a minor direct effect over *J*, but they have a structural role that is determinant in the control of the geometry of the dimetallic core and, thus, the magnetic interactions.



Scheme 2. Molecular structures of the HL and  $\text{H}_2\text{L}^{\text{S}}$  ligands. The labels P, C and S refer to specific molecular regions of these ligands.



Scheme 3. Molecular structures of the bridges found in the complexes with HL and  $\text{H}_2\text{L}^{\text{S}}$  ligands. The label B refers to particular molecular regions of these bridges.

## Results and Discussion

### Synthesis of $\text{Mn}^{\text{IV}}\text{L}$ , $\text{Fe}^{\text{III}}\text{L}$ and $\text{Cr}^{\text{III}}\text{L}$ (1–3)

Ligand HL was readily and quantitatively prepared by using a previously reported procedure under classical conditions or by applying microwave irradiation. It was not straightforward to establish the appropriate conditions for the synthesis of the corresponding dinuclear complexes. Therefore, various conditions such as the reaction composition, stoichiometry, concentration, time, pH and temperature were investigated, and the optimal conditions are reported in the Experimental Section. In general, the complexes described in this work were obtained upon reaction of the ligand in the presence or absence of a base (KOAc or pyridine) and  $\text{Mn}(\text{OAc})_2$ ,  $\text{Mn}(\text{acac})_3$ ,  $\text{FeCl}_3$  or  $\text{CrCl}_3$  in organic solvents and crystallized either by slow evaporation or by the slow diffusion of a countercurrent into the complex solution at room temperature. The reactions of two equivalents of HL with  $\text{Mn}^{\text{III}}$ ,  $\text{Cr}^{\text{III}}$  or  $\text{Fe}^{\text{III}}$  salts resulted in the corresponding  $\mu_2\text{-O}$ -bridged dinuclear neutral species, in which each metal ion is coordinated to two ligands in its deprotonated form ( $\text{L}^-$ ). The anionic benzohydrazonate form  $\text{L}^-$  results from the deprotonation of the benzohydrazonic acid tautomer of HL as testified by the bond length analysis of the solid-state structure.

The reaction of manganese(III) acetylacetonate with HL in THF followed by diffusion of  $\text{Et}_2\text{O}$  allowed the crystallization of  $[\text{Mn}_2(\mu\text{-O})_2(\text{L})_4]\cdot\text{THF}$  (1, THF = tetrahydrofuran), which is composed of two  $\text{Mn}^{\text{IV}}$  ions bridged by oxo anions that originate from residual water molecules in the THF. As the reaction occurs under anaerobic conditions, the formation of  $\text{Mn}^{\text{IV}}$  from  $\text{Mn}^{\text{III}}$  seems to arise from a dismutation reaction. Notably, this phenomenon, al-

though uncommon, have been observed previously.<sup>[12]</sup> Despite numerous efforts, the Mn<sup>II</sup> derivative(s) that should result from the disproportionation reaction have not been isolated.

Complexes [Fe<sub>2</sub>(μ-OMe)<sub>2</sub>(L)<sub>4</sub>] (**2**) and [Cr<sub>2</sub>(μ-OMe)<sub>2</sub>(L)<sub>4</sub>]·CHCl<sub>3</sub>·CH<sub>3</sub>OH (**3**) feature metal ions in the +3 oxidation state bridged by methoxo anions. The reaction of iron(III) chloride with HL in the presence of the weak base KOAc in alcoholic media led to the precipitation of **2**; one should note that high concentrations were essential for the formation of **2**. Complex **3** was prepared by the reaction of chromium(III) chloride with HL in methanol under reflux containing zinc dust (Zn) in suspension. The prior reduction of Cr<sup>III</sup> to Cr<sup>II</sup> with metallic Zn followed by air oxidation to Cr<sup>III</sup> has proved to be necessary for the formation of the dimer complex over the monomeric complex (in which the metallic centre is coordinated to three ligands). Notably, **1–3** were isolated as single crystals in good yields, and their solid-state structures are described hereafter.

### Crystal Structures of the Dinuclear HL Complexes

Selected bond lengths and angles of **1–3** are collated in Table 1. Complex **1** is composed of two six-coordinate Mn<sup>IV</sup> ions that adopt a distorted octahedral geometry (Figure 1). This dimer crystallizes in the monoclinic space group *C2/c* with *Z* = 4. The core shows one THF solvent molecule per complex. Each ion is surrounded by two μ<sub>2</sub>-oxo anions and two chelating L<sup>-</sup> ligands. The structure is highly symmetrical with a C<sub>2</sub> axis orthogonal to the plane formed by Mn, Mn', O3 and O3' that passes through the centre of it. The absence of Jahn–Teller deformation strongly supports the oxidation state +4 (vs. +3). Moreover, as both metal ions have two nitrogen atoms in axial positions, the resulting disposition of the ligands is symmetrical. According to PLATON calculations, the crystal structure is stabilized by four weak intramolecular CH...N interactions that involve the cyclopentane moieties and face imine nitrogen atoms, C24H...N3', C12H...N1' and their symmetrical counterparts.

Table 1. Selected bond lengths [Å] and angles [°] of **1–3**.

Bond/angle	Mn <sup>IV</sup> L ( <b>1</b> )	Fe <sup>III</sup> L ( <b>2</b> )	Cr <sup>III</sup> L ( <b>3</b> )
M–O1	1.948	–	–
M–O2	1.950	–	–
M–N2	2.009	–	–
M–N4	2.014	–	–
M1–O1	–	1.984	1.957
M1–O2	–	1.984	1.955
M1–N2	–	2.171	2.080
M1–N4	–	2.171	2.065
M2–O3	–	1.978	1.959
M2–O4	–	1.970	1.940
M2–N6	–	2.140	2.066
M2–N8	–	2.128	2.088
M1–μO	1.809	1.963	1.980
M2–μO	1.809	2.025	1.965
M1–M2	2.762	3.107	3.058
M1–μO–M2	99.47	102.33	101.62

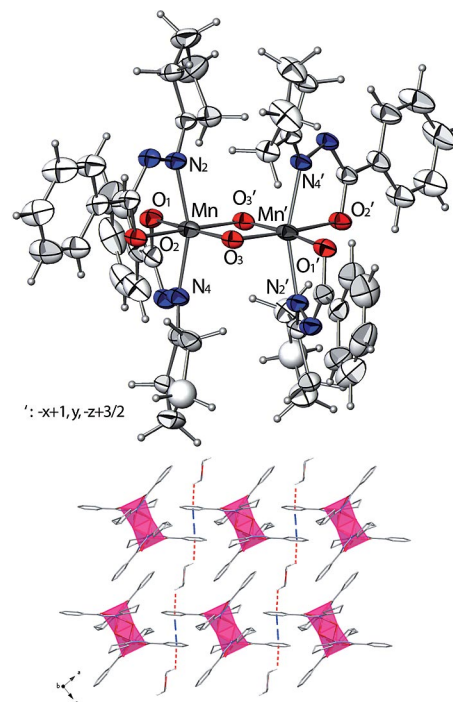


Figure 1. Top: ORTEP view of Mn<sup>IV</sup>L with partial labelling scheme; solvent molecules are omitted for clarity. Thermal ellipsoids enclose 50% of the electron density. Bottom: packing of Mn<sup>IV</sup>L in the *ac* plane; the dashed lines and the dotted lines (red) represent π–π interactions and CH–π interactions.

Complexes **2** and **3** are dinuclear species of six-coordinate Fe<sup>III</sup> and Cr<sup>III</sup> ions that crystallize in the monoclinic *P2<sub>1</sub>/a* and *P2<sub>1</sub>/c* space groups, respectively (Figures 2 and 3). Each ion is surrounded by two μ<sub>2</sub>-methoxo anions and two chelating L<sup>-</sup> ligands. In comparison with **1**, the differences arise mainly from the different oxidation states of the metal ions and the type of bridging ligands. Complexes **2** and **3** show dissymmetrical dispositions of the ligands, as one metal ion is coordinated to two nitrogen atoms in axial positions, whereas the second metal ion is coordinated to two oxygen atoms in axial positions. The coordination spheres adopt distorted octahedral geometries in which the longer M–N bonds show more deviation from the ideal octahedral geometry than the M–O bonds.

The structures of **2** and **3** slightly differ as a result of the inclusion of solvent molecules in the lattice of **3**. According to PLATON calculations, **2** is stabilized by two CH–π interactions that involve the cyclopentane moieties and face phenyl moieties C34H–Ph(C13–18) and C46H–Ph(C1–6), whereas **3** is stabilized by two weak CH–O nonclassical hydrogen bonds, C24H–O4 and C12H–O3. Finally, the structure of **2** shows that one of the CH–π interactions with the cyclopentane moiety is well defined in an envelope conformation on C46, whereas the other methylene group (CH<sub>2</sub>) involved has a very broad thermal ellipsoid. Such structural disorder could be related to the equidistant position of the CH<sub>2</sub> group between two phenyl moieties, which allows it to partake either in the CH–π interaction discussed above or

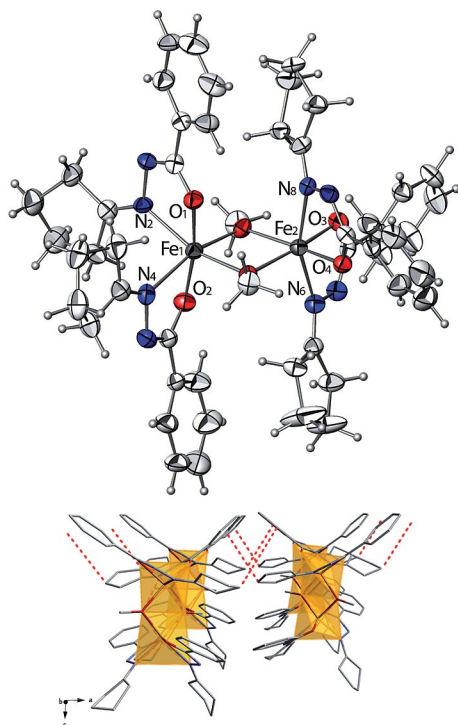


Figure 2. Top: ORTEP view of  $\text{Fe}^{\text{III}}\text{L}$  with partial labelling scheme; solvent molecules are omitted for clarity. Thermal ellipsoids enclose 50% of the electron density. Bottom: packing of  $\text{Fe}^{\text{III}}\text{L}$  in the  $ac$  plane; the dotted lines (red) represent  $\text{CH}-\pi$  interactions.

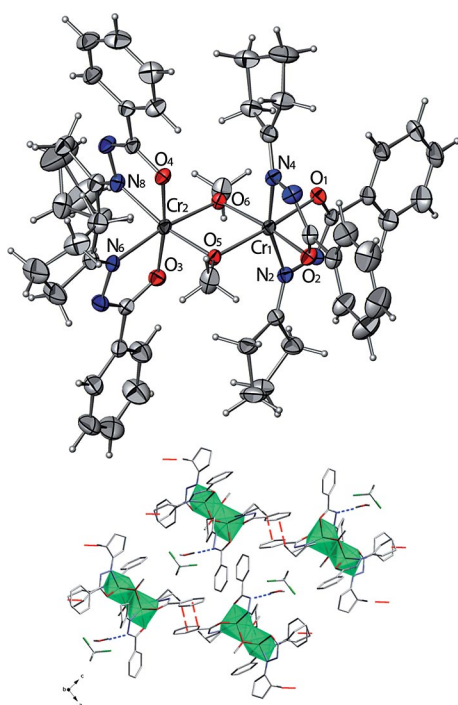


Figure 3. Top: ORTEP view of  $\text{Cr}^{\text{III}}\text{L}$  with partial labelling scheme; solvent molecules are omitted for clarity. Thermal ellipsoids enclose 50% of the electron density. Bottom: Packing of  $\text{Cr}^{\text{III}}\text{L}$  in the  $ac$  plane; H atoms are omitted for clarity, except those partaking in the represented interactions or those in solvent molecules. The dashed lines (red) represent  $\text{CH}-\pi$  interactions and the dotted lines (blue) represent H bonds.

in the intermolecular  $\text{C}34\text{H}-\text{Ph}(\text{C}25-30)$  interaction (see Solid-State Packing section).

### Solid-State Packing

As the complexes lack classical hydrogen-bond donors, their packings are driven by weaker interactions such as  $\text{CH}-\text{X}$ ,  $\pi-\pi$  and  $\text{CH}-\pi$  interactions. Complex **1** crystallizes with one THF solvent molecule and, according to PLATON calculations, shows two major intermolecular interactions that result in two interlocked  $\pi-\pi$  and  $\text{CH}-\pi$  networks in the  $ac$  plane. The  $\pi-\pi$  network arises from intermolecular interactions in which two phenyl rings stack on top of each other at 3.64 Å with a slight slippage of 0.6 Å, whereas the  $\text{CH}-\pi$  network consists of THF molecules intercalated between two phenyl rings with a  $\text{C}(\text{H})-\pi$  distance of 2.76 Å (see Figure 1). In addition, some weak  $\text{CH}-\text{X}$  interactions participate in the packing interactions.

A crossed network of intermolecular  $\text{CH}-\pi$  interactions along  $ab$  stabilizes the packing of **2**. The complex participates in the network with two phenyl  $\text{CH}$  donors and two phenyl  $\pi$ -ring acceptors with  $\text{C}(\text{H})-\pi$  distances of 3.703 and 3.814 Å, which results in closely packed layers along  $ab$ . The packing along  $c$  is derived from weak interlayer interactions, such as  $\text{CH}-\text{X}$  bonds and van der Waals interactions. In the case of **3**, the main packing interactions are the  $\text{CH}-\pi$  interactions  $\text{C}9\text{H}-\text{Ph}(\text{C}2-7)$  and  $\text{C}45\text{H}-\text{Ph}(\text{C}38-43)$  with  $\text{C}(\text{H})-\pi$  distances of 3.804 and 3.749 Å, which result in two collinear  $\text{CH}-\pi$  networks along  $b$ . The structure is further stabilized through the formation of hydrogen bonds between MeOH solvent molecules and the N3 atom of the complex.

Detailed bond lengths and angles and ORTEP views of **1**, **2** and **3** together with the powder X-ray diffraction pattern of **2** are provided in the Supporting Information.

### Computational Analysis and Validation for $\text{Mn}^{\text{III}}\text{HL}^{\text{S}}$ and $\text{Fe}^{\text{III}}\text{HL}^{\text{S}}$

The exchange coupling constant values at the CASPT2 level for the two compounds with the  $\text{H}_2\text{L}^{\text{S}}$  ligand are listed in Table 2. The reference  $J$  values for  $\text{Mn}^{\text{III}}\text{HL}^{\text{S}}$  and  $\text{Fe}^{\text{III}}\text{HL}^{\text{S}}$  are presented in the first row of Table 2 and are the result of the treatment of the electrons in the metal 3d MOs excluding any correlation effects originating in their environment. Each other row of Table 2 contains the  $J$  values obtained by activating other regions in addition to the dimetallic core. The various regions defined in the computational model incorporate the  $\pi$  system and lone pairs localized in the zones depicted in Schemes 2 and 3 (see Computational Details).

The  $J$  value obtained for  $\text{Fe}^{\text{III}}\text{HL}^{\text{S}}$  with the interactions included for all the regions is  $-22\text{ cm}^{-1}$ . This result is in very good agreement with the reported experimental value for this complex of  $-27\text{ cm}^{-1}$ [7a] and confirms the smaller impact of the ligand  $\sigma$  orbital and the diffuse MOs on the  $J$  value, as previously reported.[13] The exchange coupling

Table 2. Exchange coupling constants of the  $\text{Mn}^{\text{III}}\text{HL}^{\text{S}}$  and  $\text{Fe}^{\text{III}}\text{HL}^{\text{S}}$  compounds obtained at the CASPT2 level with the specified molecular regions enabled. The reference  $J$  values correspond to the results with all regions disabled.

Active regions <sup>[a]</sup>	$\text{Mn}^{\text{III}}\text{HL}^{\text{S}}$ $J$ [ $\text{cm}^{-1}$ ]	$\text{Fe}^{\text{III}}\text{HL}^{\text{S}}$ $J$ [ $\text{cm}^{-1}$ ]
Reference	6	-4
B	2	-9
C	5	-5
CP	5	-5
CS	5	0
CPS	4	-5
M	4	-8
BCPSM	4	-18
BCPSM+	4	-22

[a] See Schemes 2 and 3.

constant of the dimetallic core is relatively weak ( $-4 \text{ cm}^{-1}$ ), but it becomes almost eight times stronger owing to the antiferromagnetic contributions from almost all molecular regions. The only exception is the dithiolane group (S), which significantly favours the ferromagnetic coupling. The other two parts of the  $\text{H}_2\text{L}^{\text{S}}$  ligand (C and P) do not seem to have any direct effect on the magnetism of this compound. The largest antiferromagnetic contributions come from the methoxy bridges (B) and the more diffuse virtual orbitals located at the metal centres (M) and the first coordination sphere (M+). This phenomenon is not uncommon as the bridges open an indirect channel between the two metal centres that favours the antiparallel arrangement of their unpaired electrons (i.e., superexchange). Likewise, the virtual orbitals allow direct through-space interactions between the unpaired electrons of each metal centre.

On the other hand, the behaviour of  $\text{Mn}^{\text{III}}\text{HL}^{\text{S}}$  is completely insensitive to its environment. The overall  $J$  value is stable and remains ferromagnetic with a final value of  $4 \text{ cm}^{-1}$ , in good qualitative agreement with the reported ferromagnetic character of this compound ( $20 \text{ cm}^{-1}$ ).<sup>[9]</sup> Reaching quantitative agreement for ferromagnetic systems is usually complex because of specific coupling mechanisms<sup>[13]</sup> or spin polarization effects,<sup>[14]</sup> which are not included in the current CASPT2 treatment. The methoxy bridges (B) still seem to have a significant antiferromagnetic contribution, similar to that for  $\text{Fe}^{\text{III}}\text{HL}^{\text{S}}$ . However, neither the ferromagnetic effect of the dithiolane (S) nor the antiferromagnetic contribution of the virtual orbitals (M+) appear in  $\text{Mn}^{\text{III}}\text{HL}^{\text{S}}$ . These results indicate that the ferromagnetism of  $\text{Mn}^{\text{III}}\text{HL}^{\text{S}}$  is inherent to the dimetallic  $\text{Mn}^{\text{III}}/\text{Mn}^{\text{III}}$  core, and the factors that determine the  $J$  value are the relative orientation between the metal centres and the intermetallic distance. Once strong ferromagnetic coupling is achieved between the metal centres, the influence of the ligands becomes insignificant.

### Computational Results for $\text{Mn}^{\text{IV}}\text{L}$ , $\text{Fe}^{\text{III}}\text{L}$ and $\text{Cr}^{\text{III}}\text{L}$

Prompted by the robustness of our theoretical approach, we inspected the new series of compounds to anticipate their magnetic properties. Our goal is to use ab initio calcu-

lations as a tool to screen and clarify the changes in the magnetic behaviour of analogues. The exchange coupling constant values from the CASPT2 calculations performed on the three compounds with the HL ligand are shown in Table 3. The reference  $J$  values for  $\text{Mn}^{\text{IV}}\text{L}$ ,  $\text{Fe}^{\text{III}}\text{L}$  and  $\text{Cr}^{\text{III}}\text{L}$  are presented in the first row of Table 3, and only the electrons in the metal 3d MOs were treated excluding correlation effects originating in their environment. The other regions are added to the dimetallic core following the partitioning scheme shown in Schemes 2 and 3 (see Computational Details).

Table 3. Exchange coupling constant of  $\text{Mn}^{\text{IV}}\text{L}$ ,  $\text{Fe}^{\text{III}}\text{L}$  and  $\text{Cr}^{\text{III}}\text{L}$  at the CASPT2 level with the specified molecular regions enabled. The reference  $J$  values correspond to the result with all regions disabled.

Active regions <sup>[a]</sup>	$\text{Mn}^{\text{IV}}\text{L}$ (1) $J$ [ $\text{cm}^{-1}$ ]	$\text{Fe}^{\text{III}}\text{L}$ (2) $J$ [ $\text{cm}^{-1}$ ]	$\text{Cr}^{\text{III}}\text{L}$ (3) $J$ [ $\text{cm}^{-1}$ ]
Reference	-15	0	5
B	-119	-21	0
C	-32	-1	3
CP	-32	-1	3
M	-43	-4	3
BCPM	-164	-13	-1
BCPM+	-201	-17	-3

[a] See Schemes 2 and 3.

The reference magnetic character within this series of compounds with HL varies drastically from the antiferromagnetic  $\text{Mn}^{\text{IV}}\text{L}$  ( $-15 \text{ cm}^{-1}$ ) to the ferromagnetic  $\text{Cr}^{\text{III}}\text{L}$  ( $5 \text{ cm}^{-1}$ ). However, the effect that each molecular region induces on the overall  $J$  value is consistent among the three dinuclear systems 1–3. The resulting alterations of  $J$  for the dimetallic  $\text{Mn}^{\text{IV}}$ ,  $\text{Fe}^{\text{III}}$  and  $\text{Cr}^{\text{III}}$  cores is quantitatively different in absolute terms, but they show a proportional trend for all the explored regions that depends on the reference  $J$  value (see Table 3). This behaviour is equally observed for the two complexes with the  $\text{H}_2\text{L}^{\text{S}}$  ligand ( $\text{Mn}^{\text{III}}\text{HL}^{\text{S}}$  and  $\text{Fe}^{\text{III}}\text{HL}^{\text{S}}$ ), the sensitivity of which to the environment seems to be reduced by the strength of the ferromagnetic coupling between the metal centres.

The  $\text{Mn}^{\text{IV}}\text{L}$  compound is expected to have an antiferromagnetic behaviour ( $-201 \text{ cm}^{-1}$ ), one order of magnitude stronger than that of its  $\text{Fe}^{\text{III}}$  counterpart ( $-17 \text{ cm}^{-1}$ ), and the latter is also expected to be one order of magnitude more antiferromagnetic than its  $\text{Cr}^{\text{III}}$  analogue ( $-3 \text{ cm}^{-1}$ ). This ratio is maintained along the series of calculations with some moderate deviations. Therefore, it is possible to extract some common effects that these ligands produce on the three compounds. The bridging ligand (B), which is either an oxo or methoxy group, significantly increases the antiferromagnetic character of all complexes. This phenomenon is equally present for the two complexes with the  $\text{H}_2\text{L}^{\text{S}}$  ligand, but now the proportionality of this effect with the coupling of the dimetallic core (reference  $J$  value) is evidenced in the series of HL-based complexes. The diffuse virtual orbitals located at the metal centres (M) and the first coordination sphere (M+) also strengthen the antiferromagnetism of the three compounds. As observed for

the bridges, their impact on the  $J$  value is also proportional to the reference  $J$  value (see Table 3) but to a lesser extent.

The HL ligand causes a weak increase of the antiferromagnetic component that exclusively originates from the central ring (C) directly coordinated to the metal cation. The aromatic system of the phenyl group (P) is inert with respect to the exchange coupling of the molecule. As HL does not have the dithiolane group (S), which induces a ferromagnetic contribution for the  $H_2L^S$  complexes, it could be expected that HL would exhibit a stronger antiferromagnetic contribution in comparison. The clearest example is the  $Mn^{IV}L$  compound, the  $J$  value of which becomes twice as antiferromagnetic with the CP regions activated. Unfortunately, the  $J$  values of the other compounds are too small to allow any conclusion about this matter.

Furthermore, the alterations of  $J$  induced by the different regions are additive for  $Mn^{IV}L$  complex but not for  $Fe^{III}L$  and  $Cr^{III}L$ . The  $J$  value of the  $Mn^{IV}L$  system with the BCPM region active is  $-164\text{ cm}^{-1}$ , and the sum of the independent contributions of the B, CP and M regions to the reference value is exactly  $-164\text{ cm}^{-1}$ . The contribution of a certain region can be obtained by subtracting the reference  $J$  value from the  $J$  of the region. However, this is not the case for  $Fe^{III}L$ , which experiences an antiferromagnetic contribution of  $-13\text{ cm}^{-1}$  with the BCPM region enabled, whereas the sum of the individual components accounts for double that ( $-26\text{ cm}^{-1}$ ). A similar behaviour is observed for the Cr complex, which has a  $J$  value of  $-1\text{ cm}^{-1}$  with BCPM and  $-6\text{ cm}^{-1}$  for the sum of the parts. The combined interactions between the individual regions are definitely not equivalent between the  $Mn^{IV}$  system and the  $Fe^{III}$  and  $Cr^{III}$  compounds. This distinct behaviour could be related to their bridge ligands, which are oxo for  $Mn^{IV}L$  and methoxo for  $Fe^{III}L$  and  $Cr^{III}L$ . Nevertheless, it is difficult to affirm whether this change is due solely to the different interaction of the bridges or also to the character of the involved metal centres.

## Conclusions

We have developed a computational strategy based on ab initio CASPT2 calculations that uses localized orbitals and is capable of selectively enabling or disabling different regions of the molecule. This technique has been applied to analyze the specific influence on the exchange coupling constant of various dinuclear transition metal compounds with aroylhydrazone ligands.

The calculated  $J$  values for the two complexes with the  $H_2L^S$  ligand are in good agreement with the experimental ones,  $J = 4\text{ cm}^{-1}$  for  $Mn^{III}HL^S$  and  $J = -22\text{ cm}^{-1}$  for  $Fe^{III}HL^S$ . The influence of the various molecular regions (Scheme 2) over  $J$  shows that the different contributions to the overall magnetism largely depend on the inherent intermetallic coupling (Table 2). The ferromagnetic complex  $Mn^{III}HL^S$  is not significantly affected by the interaction with the  $H_2L^S$  ligands and the bridges, whereas the antiferromagnetic  $Fe^{III}HL^S$  complex exhibits a wider range of ef-

fects induced by its environment. The strongest contributions are antiferromagnetic and come from the bridges (superexchange) and the virtual orbitals localized around the metal centres (direct exchange). Notably, the dithiolane group significantly increases the ferromagnetic component of the system. Nonetheless, the  $H_2L^S$  ligand has minor electronic interactions with the dimetallic core and, thus, it directs the magnetic properties of the compound by conditioning the relative arrangement of the metal centres (the M–M distance and M– $\mu$ OMe–M angles). Usually, exchange coupling constants involving metal centres are strongly sensitive to small distortions of the metallic coordination sphere.<sup>[15]</sup> One example is the different  $J$  value obtained when the B regions are activated for  $Fe^{III}HL^S$  ( $-9\text{ cm}^{-1}$ ) and  $Fe^{III}L$  ( $-21\text{ cm}^{-1}$ ), which have a chemically equivalent dimetallic core. Unfortunately, the analysis of this behaviour involves too many structural parameters to be addressed in the present work.

Three dinuclear complexes with the HL ligand (1–3) have been synthesized and fully characterized, and their solid-state structures have been elucidated by X-ray diffraction crystallography. These systems extend the series of compounds with the HL ligand, which is chemically simpler than  $H_2L^S$ . All three complexes are expected to be antiferromagnetic with  $J = -201\text{ cm}^{-1}$  for  $Mn^{IV}L$ ,  $J = -17\text{ cm}^{-1}$  for  $Fe^{III}L$  and  $J = -3\text{ cm}^{-1}$  for  $Cr^{III}L$  (Table 3). The behaviour of these compounds is very similar to that of  $Mn^{III}HL^S$  and  $Fe^{III}HL^S$ . Their strongest contributions are equally antiferromagnetic and arise from the bridges and the virtual orbitals localized around the metal centres. Nonetheless, the series of compounds based on HL show a clearer dependency of these antiferromagnetic contributions to the inherent intermetallic coupling. The larger the ferromagnetic coupling between the metal centres (reference  $J$  value), the less affected is the overall magnetism by the superexchange and direct exchange. Therefore, the control of the overall magnetism that the HL ligand imposes by determining the structure of the dimetallic core is more effective than any external electronic interaction. The HL ligand has the capacity to control the reference  $J$  and, hence, the extent of the antiferromagnetic superexchange and direct exchange effects. However, if the inherent ferromagnetism of the dimetallic core is not sufficiently large, these effects could still switch the complex to (slightly) antiferromagnetic behaviour.

As the dinuclear  $Mn^{III}$  complexes can present a ferromagnetic exchange interaction in favourable circumstances, our current investigation aims to include other bridging ligands as well as find a synthetic strategy that could prevent the in situ oxidation of  $Mn^{III}$  to  $Mn^{IV}$ .

## Experimental Section

**Syntheses of the Organic and Metallorganic Compounds:** Unless otherwise stated, manipulations were performed under anaerobic conditions (Ar) by using standard Schlenk techniques. Commercial reagents were used as purchased, and solvents were degassed prior

to use. IR spectra were recorded with a Nicolet 380 FTIR spectrometer. The yields of **1–3** are those of isolated crystals.

**Ligand HL:** Benzohydrazide (5 g, 36.7 mmol) and cyclopentanone (3.09 g, 36.7 mmol, 1 equiv.) were placed in a quartz tube, which was placed in a microwave oven and heated at 200 W for 3 min. Then, the resulting mixture was cooled to room temperature. After the addition of Et<sub>2</sub>O (20 mL) and further washing with Et<sub>2</sub>O (4 × 15 mL), HL was isolated as a white solid (quantitative). <sup>1</sup>H NMR (400 MHz, [D<sub>6</sub>]DMSO): δ = 1.70–1.78 (m, 4 H), 2.30–2.48 (m, 4 H), 7.48 (d, 2 H, *J* = 6.5 Hz), 7.54 (d, 1 H, *J* = 6.1 Hz), 7.81 (d, 2H *J* = 5.6 Hz), 10.29 (s, 1 H) ppm. <sup>13</sup>C NMR (100 MHz, [D<sub>6</sub>]DMSO): δ = 24.2, 24.3, 28.5, 33.0, 127.6, 128.2, 131.2, 134.1, 163.2, 170.2 ppm. All analyses are in agreement with those previously reported.<sup>[16]</sup>

**[Mn<sup>IV</sup><sub>2</sub>(μ-O)<sub>2</sub>(L)<sub>4</sub>]·THF (1):** Mn(acac)<sub>3</sub> (174 mg, 0.5 mmol) was added to a stirred solution of HL (200 mg, 1 mmol, 2 equiv.) in THF (20 mL). The mixture was further stirred for 24 h at room temp. and then concentrated under reduced pressure. Slow diffusion of Et<sub>2</sub>O into the THF solution afforded black crystals suitable for X-ray diffraction analysis in 5 d, yield 30% (based on Mn). IR: ν̄ = 1638, 1588, 1517, 1491, 1443, 1405, 1361, 1172, 1136, 1068, 1026, 995, 940, 791, 707, 689, 667 cm<sup>-1</sup>. C<sub>48</sub>H<sub>56</sub>Mn<sub>2</sub>N<sub>8</sub>O<sub>6</sub>·THF: calcd. C 61.29, H 5.93, N 10.99; found C 60.93, H 5.89, N 10.90.

**[Fe<sup>III</sup><sub>2</sub>(μ-OMe)<sub>2</sub>(L)<sub>4</sub>] (2):** A solution of FeCl<sub>3</sub>·6H<sub>2</sub>O (16 mg, 0.1 mmol) in MeOH (2 mL) was added to a stirred solution of HL (40 mg, 0.2 mmol, 2 equiv.) in MeOH (2 mL). Then, a solution of KOAc (20 mg, 0.2 mmol, 2 equiv.) in MeOH (2 mL) was added dropwise to the resulting mixture. The mixture was stirred for 1 h at room temp. A red precipitate formed and was separated by filtration and dissolved in CHCl<sub>3</sub> (5 mL). Slow diffusion of MeOH into the CHCl<sub>3</sub> solution gave red crystals suitable for X-ray diffraction analysis in 4 d, yield 18% (based on Fe). IR: ν̄ = 1634, 1587, 1519, 1491, 1439, 1410, 1369, 1358, 1212, 1171, 1137, 1068, 1038, 1028, 992, 936, 791, 759, 709, 679, 668 cm<sup>-1</sup>. C<sub>50</sub>H<sub>58</sub>Fe<sub>2</sub>N<sub>8</sub>O<sub>6</sub> (978.75): calcd. C 61.36, H 5.97, N 11.45; found C 61.11, H 6.10, N 11.34.

**[Cr<sup>III</sup><sub>2</sub>(μ-OMe)<sub>2</sub>(L)<sub>4</sub>]·CHCl<sub>3</sub>·MeOH (3):** CrCl<sub>3</sub> (32 mg, 0.2 mmol) and HL (83 mg, 0.4 mmol, 2 equiv.) were sequentially added to a stirred suspension of Zn dust (220 mg, 33 mmol) in MeOH (20 mL). The resulting mixture was heated at reflux for 24 h, cooled to room temp. and then evaporated to dryness. The resulting black powder was dissolved in CH<sub>2</sub>Cl<sub>2</sub> (10 mL), and the solution was filtered through Celite. Slow evaporation of a 1:1 MeOH/CHCl<sub>3</sub> mixture (2 mL) gave black crystals suitable for X-ray diffraction analysis in 2 d, yield 10% (based on Cr).

C<sub>50</sub>H<sub>58</sub>Cr<sub>2</sub>N<sub>8</sub>O<sub>6</sub>·CH<sub>3</sub>OH·CHCl<sub>3</sub>: calcd. C 55.64, H 5.66, N 9.98; found C 55.23, H 5.74, N 9.83.

**X-ray Crystallography:** Single crystal X-ray diffraction measurements were performed at 173 K by using a Nonius Kappa CCD or a Bruker APEX-II CCD diffractometer with Mo-*K*<sub>α</sub> radiation. The crystal structures were solved by direct methods and refined by employing full-matrix least-squares on *F*<sup>2</sup> (SHELXL-97). All non-hydrogen atoms were refined anisotropically, and the hydrogen atoms of organic ligands were introduced by using a riding model (SHELXL-97). Crystal data and refinement details of the structure determination for **1–3** are listed in Table 4. CCDC-941599 (for **1**), -941600 (for **2**) and -941601 contain the supplementary crystallographic data for this paper. These data can be obtained free of charge from The Cambridge Crystallographic Data Centre via www.ccdc.cam.ac.uk/data\_request/cif.

**Computational Details:** The exchange coupling constant (*J*) has been calculated for the two dinuclear complexes with the H<sub>2</sub>L<sup>S</sup> ligand (i.e., Mn<sup>III</sup>HLS, Fe<sup>III</sup>HLS) and the three complexes with HL (i.e., Mn<sup>IV</sup>L, Fe<sup>III</sup>L, Cr<sup>III</sup>L). We used the molecular structures derived from the X-ray data without any further computational geometrical refinement or chemical simplification. The crystallographic structures of Mn<sup>IV</sup>L, Fe<sup>III</sup>L and Cr<sup>III</sup>L are provided in the present work, whereas the solid-state structures of Mn<sup>III</sup>HLS and Fe<sup>III</sup>HLS are available in ref.<sup>[9]</sup> and ref.<sup>[7a]</sup>, respectively. The electronic structure of a single molecule in vacuo was obtained from ab initio calculations by using the CASPT2 method.<sup>[10]</sup> We calculated the low-spin (LS) state and the high-spin (HS) state for each complex. As all systems have a dimetallic magnetic centre with a maximum spin multiplicity larger than *S* = 1/2, for the sake of simplicity, we chose to work with the highest spin state available instead of the triplet state. For the diiron compounds, there are two Fe<sup>III</sup>(3d<sup>5</sup>) centres that generate an undecuplet HS state (*S* = 5). The ferromagnetic Mn<sup>III</sup>HLS has two Mn<sup>III</sup>(3d<sup>4</sup>) centres that give rise to a nonuplet HS state (*S* = 4). On the other hand, the Cr<sup>III</sup>L and Mn<sup>IV</sup>L complexes have two Cr<sup>III</sup>(3d<sup>3</sup>) and two Mn<sup>IV</sup>(3d<sup>3</sup>) centres, respectively, and their HS state is a septuplet (*S* = 3). In all cases, the LS state is a singlet state. Therefore, we can extract *J* from the difference in energy between each pair of HS/LS states. From the Heisenberg Hamiltonian model  $\hat{H} = -J\sum_i \hat{S}_i \hat{S}_{i+1}$ , the HS/LS difference for the diiron compounds accounts for 15*J* = *E*<sub>LS</sub> - *E*<sub>HS</sub>, whereas for the Mn<sup>III</sup>HLS system it is 10*J*, and for both Cr<sup>III</sup>L and Mn<sup>IV</sup>L complexes it is 6*J*.

The CASPT2 method performs a perturbational expansion on top of a zero-order complete active space self-consistent field (CASSCF) Hamiltonian.<sup>[10]</sup> This CASSCF reference defines an

Table 4. Crystal data and refinement details of **1–3**.

	Mn <sup>IV</sup> L (1)	Fe <sup>III</sup> L (2)	Cr <sup>III</sup> L (3)
Formula	C <sub>48</sub> H <sub>52</sub> Mn <sub>2</sub> N <sub>8</sub> O <sub>6</sub> ·THF	C <sub>50</sub> H <sub>58</sub> Fe <sub>2</sub> N <sub>8</sub> O <sub>6</sub>	C <sub>50</sub> H <sub>58</sub> Cr <sub>2</sub> N <sub>8</sub> O <sub>6</sub> ·MeOH·CHCl <sub>3</sub>
Fw	1018.97	978.75	1122.47
Space group	<i>C2/c</i>	<i>P2<sub>1</sub>/a</i>	<i>P2<sub>1</sub>/c</i>
<i>a</i> [Å]	18.0900(10)	18.9370(6)	21.300(0)
<i>b</i> [Å]	17.3950(11)	11.3680(5)	10.796(8)
<i>c</i> [Å]	15.2690(7)	22.5530(6)	23.491(0)
β [°]	92.853(3)	93.555(2)	97.114(0)
<i>Z</i>	4	4	4
<i>T</i> [K]	173	173	173
λ (Mo- <i>K</i> <sub>α</sub> ) [Å]	0.71073	0.71073	0.71073
Calculated density (g cm <sup>-3</sup> )	1.410	1.342	1.391
μ (Mo- <i>K</i> <sub>α</sub> ) [cm <sup>-1</sup> ]	5.88	6.56	6.13
<i>R</i> <sub>1</sub> and <i>R</i> <sub>w</sub> [ <i>I</i> > 2σ( <i>I</i> )] <sup>[a]</sup>	0.0717, 0.1744	0.1086, 0.2439	0.0727, 0.1921

[a]  $R_1 = \sum (|F_o| - |F_c|) / \sum |F_o|$ .  $R_w = [\sum w(F_o^2 - F_c^2)^2 / \sum w(F_o^2)^2]^{1/2}$ .  $w = 1 / [\sigma^2(F_o^2) + (np)^2 + 0.00p]$ ,  $p = \max(F_o^2) + (2F_c^2)/3$ .

active space (CAS) of molecular orbitals (MO) and incorporates all the allowed electronic excitations within the CAS into the wave function. The dimetallic complexes under study have open 3d shells on both metal centres. Therefore, to produce a balanced description of the LS and HS states for all dinuclear complexes, we defined a CAS formed by the ten 3d-like MOs. The active space for the diiron compounds incorporates ten 3d electrons for a total CAS[10,10]. Analogously, the  $\text{Mn}^{\text{III}}\text{HL}^{\text{S}}$  system employed a CAS[8,10] with eight 3d electrons for both  $\text{Mn}^{\text{III}}$  atoms. The active space employed for the  $\text{Cr}^{\text{III}}\text{L}$  and  $\text{Mn}^{\text{IV}}\text{L}$  complexes is a CAS[6,10]. The LS and HS calculations of the five systems were performed by solving, in each case, one electronic state with the corresponding spin multiplicity. All the electronic structure calculations were performed with the MOLCAS7 package.<sup>[17]</sup>

We analyzed the influence of the coordination sphere and the different parts of the ligands on the magnetic properties of the complexes. Once we achieved a good qualitative description of both systems at the CASSCF level, we applied the CASPT2 step locally to some regions of the molecule and incorporated selectively the so-called dynamical correlation. This procedure is based on the localization of the delocalized MO set resulting from the CASSCF calculation.<sup>[18]</sup> The orbitals are transformed by following a valence-bond-like description of the electronic density, which is based on one of the Kekulé structures of the molecule and allows us to spatially separate the orbitals.<sup>[19]</sup> Once the partitioning is done, it becomes possible to enable/disable defined regions of the compound (e.g., the bridges between the metal centres or some aromatic rings) to analyze how they affect the magnetic properties of the molecule. We used the DOLO set of tools, which are available in the CASDI code,<sup>[20]</sup> to perform the localization.

The schemes of the partition are shown in Schemes 2 and 3. It must be noted that the regions established for the partitioning do not contain all the electronic density localized on them. We always left the core orbitals and the  $\sigma$ -type orbitals disabled, specifically, as frozen for the occupied MOs or deleted for the virtual MOs in the CASPT2 calculation, because this type of orbitals is largely nonpolarizable and will not interact with the metal centres.<sup>[21]</sup> Thus, the partition was performed upon the  $\pi$ -type MOs and the nonbonding MOs. Tables 5 and 6 show the exact distribution of orbitals over the different partition stages. Additionally, diffuse virtual orbitals located on the metal centres (M) and its coordination sphere (M+) are also enabled at a later stage to analyze their influence on the magnetic properties.

Table 5. Number and type of molecular orbitals constituting each of the regions defined on the partitioning for  $\text{Mn}^{\text{III}}\text{HL}^{\text{S}}$  and  $\text{Fe}^{\text{III}}\text{HL}^{\text{S}}$ . A schematic representation of the spatial limits of each region can be found in Schemes 2 and 3.

Region	Type of molecular orbital			
	<i>n</i>	$\pi$	$\pi^*$	Diffuse
B	6	0	0	0
C	20	8	8	0
CP	28	20	20	0
CS	36	8	8	0
CPS	44	20	20	0
M	0	0	0	82
BCPSM	50	20	20	82
BCPSM+ 50	20	20	20	270

We used the molecular structures obtained from the X-ray data of the respective crystalline systems. All the atoms of the molecule are described with ANO-RCC type basis sets.<sup>[22]</sup> The metal centres have a basis set formed by 6s5p4d2f contracted functions, the O

Table 6. Number and type of molecular orbitals constituting each of the regions defined on the partitioning for  $\text{Mn}^{\text{IV}}\text{L}$ ,  $\text{Fe}^{\text{III}}\text{L}$  and  $\text{Cr}^{\text{III}}\text{HL}$ . A schematic representation of the spatial limits of each region can be found in Schemes 2 and 3.

Region	Type of molecular orbital			
	<i>n</i>	$\pi$	$\pi^*$	Diffuse
B	6 <sup>[a]</sup>	0	0	0
C	20	8	8	0
CP	20	20	20	0
M	0	0	0	82
BCPM	26 <sup>[a]</sup>	20	20	82
BCPM+	26 <sup>[a]</sup>	20	20	212

[a] Two more MOs for the  $\text{Mn}^{\text{IV}}\text{L}$  complex.

and N atoms have a set of 4s3p1d contracted functions, the C atoms have a 3s2p set of contracted functions, and the H atoms have a 2s basis set. We took advantage of the Cholesky decomposition to reduce the computational cost of working with these relatively large molecules.<sup>[23]</sup> We performed the CASPT2 calculations with an IPEA value of 0.00 hartree. This original choice of the zeroth-order Hamiltonian gives more accurate results for magnetic coupling parameters than the modified Hamiltonian.<sup>[24]</sup> We also had to apply an imaginary shift factor of 0.20 hartree for the CASPT2 step,<sup>[25]</sup> which we previously tested to be the minimum value to eliminate possible intruder states.

**Supporting Information** (see footnote on the first page of this article): Detailed bond lengths and angles, ORTEP views of 1–3, powder X-ray diffraction pattern of 2.

## Acknowledgments

This work was supported by the Centre National de la Recherche Scientifique (CNRS). A. D. and V. R. thank the Agence Nationale de la Recherche (ANR) (project number ANR-2010-BLAN-703) and the Excellence Network Chemistry of Complex Systems (LabEx CSC, ANR-10-LABX-0026\_CSC) for financial support. D. S., S. M. and R. W. thank the Ministère de la Recherche (France) for PhD financial support. V. R. thanks the Fundação para a Ciência e Tecnologia (FCT) for the funding of a fellowship (SFRH/BPD/44262/ 2008).

- [1] a) C. J. Ballhausen, *Introduction to Ligand Field Theory*, McGraw-Hill, New York, **1962**, p. 298; b) M. Atanasov, D. Ganyushin, K. Sivalingam, F. Neese, in: *Structure and Bonding* vol. 142: *Molecular Electronic Structures of Transition Metal Complexes II* (Eds.: D. M. P. Mingos, P. Day, J. P. Dahl), Springer, Berlin, **2012**, p. 149–220.
- [2] O. Kahn, *Molecular Magnetism*, Wiley-VCH, New York, **1993**, p. 396.
- [3] a) K. R. Reddy, M. V. Rajasekharan, S. Padhye, F. Dahan, J. P. Tuchagues, *Inorg. Chem.* **1994**, *33*, 428; b) N. K. Thallaj, J. Przybilla, R. Welter, D. Mandon, *J. Am. Chem. Soc.* **2008**, *130*, 2414.
- [4] a) R. E. P. Winpenny, *Structure and Bonding*, vol. 122: *Single-Molecule Magnets and Related Phenomena*, Springer, Berlin, **2006**, p. 262; b) A. Caneschi, D. Gatteschi, R. Sessoli, A. L. Barra, L. C. Brunel, M. Guillot, *J. Am. Chem. Soc.* **1991**, *113*, 5873; c) R. Sessoli, *Mol. Cryst. Liq. Cryst. Sci. Technol., Sect. A* **1995**, *274*, 145; d) D. Gatteschi, R. Sessoli, *Angew. Chem. Int. Ed.* **2003**, *42*, 268; *Angew. Chem.* **2003**, *115*, 278.
- [5] a) M. N. Leuenberger, D. Loss, *Nature* **2001**, *410*, 789; b) A. R. Rocha, V. M. García-suárez, S. W. Bailey, C. J. Lambert, J. Ferrer, S. Sanvito, *Nat. Mater.* **2005**, *4*, 335; c) F. Troiani, A. Ghirri, M. Affronte, S. Carretta, P. Santini, G. Amoretti, S.

- Piligkos, G. Timco, R. E. P. Winpenny, *Phys. Rev. Lett.* **2005**, *94*, 207208; d) L. Bogani, W. Wernsdorfer, *Nat. Mater.* **2008**, *7*, 179; e) G. A. Timco, S. Carretta, F. Troiani, F. Tuna, R. J. Pritchard, C. A. Muryn, E. J. L. McInnes, A. Ghirri, A. Candini, P. Santini, G. Amoretti, M. Affronte, R. E. P. Winpenny, *Nat. Nanotechnol.* **2009**, *4*, 173.
- [6] a) K. Mogilaiah, M. Prashanthi, G. Randheer Reddy, *Synth. Commun.* **2003**, *33*, 3741; b) G. I. Mustata, A. Brigo, J. M. Briggs, *Bioorg. Med. Chem. Lett.* **2004**, *14*, 1447; c) L. Saiz-Urra, M. P. González, Y. Fall, G. Gómez, *Eur. J. Med. Chem.* **2007**, *42*, 64; d) K. Mogilaiah, E. Anitha, K. S. Kumar, R. S. Prasad, *Ind. J. Chem. B* **2011**, *50*, 126; e) V. F. Shul'gin, E. A. Sarnit, O. V. Konnik, E. B. Rusanov, A. S. Bogomyakov, V. I. Ovcharenko, V. V. Minin, *Russ. J. Coord. Chem.* **2012**, *38*, 44.
- [7] a) N. Bouslimani, N. Clément, G. Rogez, P. Turek, M. Bernard, S. Dagorne, D. Martel, H. N. Cong, R. Welter, *Inorg. Chem.* **2008**, *47*, 7623; b) N. Clément, C. Toussaint, G. Rogez, C. Loose, J. Kortus, L. Brelot, S. Choua, S. Dagorne, P. Turek, R. Welter, *Dalton Trans.* **2010**, *39*, 4579; c) D. Specklin, C. Tourbillon, V. Rosa, M. Kurmoo, R. Welter, *Inorg. Chem. Commun.* **2012**, *20*, 172; d) W. Zuo, V. Rosa, C. Tourbillon, D. Specklin, C. Khaled, M. Kurmoo, R. Welter, *RSC Adv.* **2012**, *2*, 2517.
- [8] a) R. Welter, WO 2009/130562 A1, **2009**; b) K. Cheaib, D. Martel, N. Clément, F. Eckes, S. Kouaho, G. Rogez, S. Dagorne, M. Kurmoo, S. Choua, R. Welter, *Dalton Trans.* **2013**, *42*, 1406.
- [9] C. Beghidja, G. Rogez, J. Kortus, M. Wesolek, R. Welter, *J. Am. Chem. Soc.* **2006**, *128*, 3140.
- [10] a) B. O. Roos, P. R. Taylor, P. E. M. Siegbahn, *Chem. Phys.* **1980**, *48*, 157; b) K. Andersson, P. A. Malmqvist, B. O. Roos, A. J. Sadlej, K. Wolinski, *J. Phys. Chem.* **1990**, *94*, 5483; c) K. Andersson, P.-Å. Malmqvist, B. O. Roos, *J. Chem. Phys.* **1992**, *96*, 1218.
- [11] a) K. Pierloot, E. Van Praet, L. G. Vanquickenborne, B. O. Roos, *J. Phys. Chem.* **1993**, *97*, 12220; b) C. de Graaf, R. Broer, W. C. Nieuwpoort, *Chem. Phys.* **1996**, *208*, 35.
- [12] K. Wiegardt, U. Bossek, B. Nuber, J. Weiss, J. Bonvoisin, M. Corbella, S. E. Vitols, J. J. Girerd, *J. Am. Chem. Soc.* **1988**, *110*, 7398.
- [13] a) O. Oms, J.-B. Rota, L. Norel, C. J. Calzado, H. Rousselière, C. Train, V. Robert, *Eur. J. Inorg. Chem.* **2010**, 5373; b) J.-B. Rota, C. J. Calzado, C. Train, V. Robert, *J. Chem. Phys.* **2010**, *132*, 154702.
- [14] A. Domingo, M. Vérot, F. Mota, C. de Graaf, J. J. Novoa, V. Robert, *Phys. Chem. Chem. Phys.* **2013**, *15*, 6982.
- [15] A.-M. Pradipto, R. Maurice, N. Guihéry, C. de Graaf, R. Broer, *Phys. Rev. B* **2012**, *85*, 014409.
- [16] M. M. Andrade, M. T. Barros, *J. Comb. Chem.* **2010**, *12*, 245.
- [17] F. Aquilante, L. De Vico, N. Ferré, G. Ghigo, P.-Å. Malmqvist, P. Neogrády, T. B. Pedersen, M. Pitoňák, M. Reiher, B. O. Roos, L. Serrano-Andrés, M. Urban, V. Veryazov, R. Lindh, *J. Comput. Chem.* **2010**, *31*, 224.
- [18] a) S. F. Boys, *Rev. Mod. Phys.* **1960**, *32*, 296; b) J. Pipek, P. G. Mezey, *J. Chem. Phys.* **1989**, *90*, 4916; c) C. Angeli, G. Del Re, M. Persico, *Chem. Phys. Lett.* **1995**, *233*, 102.
- [19] a) J.-P. Malrieu, N. Guihéry, C. J. Calzado, C. Angeli, *J. Comput. Chem.* **2007**, *28*, 35; b) C. J. Calzado, C. Angeli, D. Taratiel, R. Caballol, J.-P. Malrieu, *J. Chem. Phys.* **2009**, *131*, 044327; c) J. Zapata-Rivera, R. Caballol, C. J. Calzado, *Phys. Chem. Chem. Phys.* **2011**, *13*, 20241.
- [20] N. Ben Amor, D. Maynau, *Chem. Phys. Lett.* **1998**, *286*, 211.
- [21] T. Heine, R. Islas, G. Merino, *J. Comput. Chem.* **2007**, *28*, 302.
- [22] a) B. O. Roos, R. Lindh, P.-Å. Malmqvist, V. Veryazov, P.-O. Widmark, *J. Phys. Chem. A* **2004**, *108*, 2851; b) B. O. Roos, R. Lindh, P.-Å. Malmqvist, V. Veryazov, P.-O. Widmark, *J. Phys. Chem. A* **2005**, *109*, 6575.
- [23] F. Aquilante, P.-Å. Malmqvist, T. B. Pedersen, A. Ghosh, B. O. Roos, *J. Chem. Theory Comput.* **2008**, *4*, 694.
- [24] N. Queralt, D. Taratiel, C. de Graaf, R. Caballol, R. Cimiraglia, C. Angeli, *J. Comput. Chem.* **2008**, *29*, 994.
- [25] N. Forsberg, P.-Å. Malmqvist, *Chem. Phys. Lett.* **1997**, *274*, 196.

Received: February 19, 2014  
Published Online: April 23, 2014